

Separation of Mass-Overlapped Time of Flight-Energy Elastic Recoil Detection Analysis Data Using Ryan and Jamieson's Dynamic Analysis Method

Leif Persson,^{a,*} Harry J. Whitlow,^{a,†} Mohamed El Bouanani,^{a,**} Mikael Hult,^{a,*} Margaretha Andersson,^b Ian F. Bubb,^c David D. Cohen^d, Nick Dytlewski^d, Peter N. Johnston,^c Scott R. Walker,^{c***} Carina Zaring,^{e****} Mikael Östling^e

^a *Division of Nuclear Physics, Lund Institute of Technology, Box 118, S-221 00 Lund, Sweden*

^b *Department of Inorganic Chemistry, Ångström Laboratory, Uppsala University, Box 538, S-751 21 Uppsala, Sweden*

^c *Department of Applied Physics, Royal Melbourne Institute of Technology, GPO Box 2476V, Melbourne 3001, Australia*

^d *Australian Nuclear Science and Technology Organisation, PMB 1, Menai 2234, Australia*

^e *Department of Electronics, Device Component Laboratory, Royal Institute of Technology, P.O. Box Electrum 229, S-164 40 Kista, Sweden*

Abstract

Time of Flight-Energy Elastic Recoil Detection Analysis (ToF-E ERDA) data often contains mass signals with considerable overlap from adjacent isotopes in the mass-energy plane. An evaluation has been carried out of the suitability of the dynamic analysis method proposed by Ryan and Jamieson to decompose elemental signals with overlapping mass. The method is shown to work very well on generated test data and the result when it was applied to experimental data appears quite promising. Very accurate mass calibration and lineshape determination was found to be a prerequisite for the application of the method.

PACS:29.30.Ep, 82.80.Yc, 02.50.Wp

[†] **Corresponding Author:** e-mail Harry.J.Whitlow@nuclear.lu.se, tel +46-46-222 7630, fax +46-46-222 4709

* Present address: CEC-JRC-IRMM, Retieseweg, B-2440 Geel, Belgium

** Present address: Ion Beam Modification and Analysis Laboratory, Department of Physics, University of North Texas, Denton Texas 76203-5307, USA.

*** Present address: Weapons Systems Division, Defence Science and Technology Organisation, P.O. Box 1500, Salisbury, SA, 5108, Australia.

**** Present address: Ericsson Microelectronics AB, SE-164 81 Kista, Sweden

1. Introduction

Elastic Recoil Detection Analysis (ERDA) using high energy heavy ions as the probing beam has found significant application for the study of thin-film structures with elements with mass number A in the range 50-120, e.g. metal/III-V semiconductor contacts [1], ferrous alloys [1] as well as magnetic [2,3] and optical [4] thin film information storage media. To determine the energy and the identity of each recoiling atom and its depth of origin a ΔE -E detection system or a detector telescope instrumented to measure the Time of Flight (ToF) and Energy can be employed. The data can be represented as a two-dimensional histogram of (ΔE vs. E) or (ToF vs. E) in these cases. It is often preferable to map the data into a two-dimensional histogram of Z vs. E [5-9] or A vs. E [10,11], respectively. The signals from different elements are then distributed about isobaric or isotopic lines in the histogram. By carefully selecting the gates for each element (isotope) it is possible to minimise the cross talk from other near-lying elements (isotopes) [11-14]. However, the approach has a number of inherent disadvantages:

- (i) Data is discarded in regions where the cross talk is large.
- (ii) Signals from elements with overlapping isotopes are difficult to handle.
- (iii) Non-linearity in the Si E-detector response [10,15] leads to a curving of the data point distribution on an A vs. E histogram away from the ideal straight constant mass line for a particular isotope.

The latter disadvantage can, to some degree, be overcome by calibration of the E detector, e.g. for a ToF-E detector telescope by using a multivariate least squares fitting procedure [10]. However, (i) and (ii) require that a complete spectral decomposition [16-18] or two-dimensional simulation procedure [19] be used.

Ryan and Jamieson [20-23] have proposed a dynamic statistical method, which can be used for on-line overlap-resolved elemental mapping in PIXE-microprobe measurements. The method performs spectral analysis by using linear fitting to X-ray spectra where normally non-linear least-square fitting is used. The method is based on a matrix multiplication, which describes how much an X-ray photon with a particular energy contributes to the signal for each element. The transformation matrix can be determined experimentally from calibration standards, or calculated from known energies and line-widths. This method is potentially much faster than conventional non-linear fitting because once the transformation matrix has been established, the transformation is a simple matrix multiplication rather than an iterative minimisation algorithm and it may thus be applied concurrently to a large number of samples. Moreover, once the transformation matrix has been established the procedure can be used for on-line monitoring of the energy spectra from different elements during the measurement.

2. Basis of the Numerical Method

Following Ryan and Jamieson [20-23] consider a one-dimensional spectrum vector \mathbf{S} with channel contents S_i and associated statistical weight w_i . The least squares fit of a function

$f_i(\mathbf{a}, i)$ that is linear in its parameters a_k can be written in the form of the matrix equation:

$$\mathbf{a}\mathbf{a} = \mathbf{b}\mathbf{S}$$

where \mathbf{a} is the vector of adjustable parameters a_k and the matrices \mathbf{a} and \mathbf{b} have elements:

$$a_{jk} = \sum_i w_i^{-1} \mathbf{b}_{ji} \mathbf{b}_{ki}$$

$$\mathbf{b}_{ji} = w_i \left(\frac{\partial f_i(\mathbf{a}, i)}{\partial a_j} \right)$$

The vector \mathbf{a} is then from eqn. 1 given by:

$$\mathbf{a} = \mathbf{a}^{-1} \hat{\mathbf{a}} \mathbf{S} = \tilde{\mathbf{A}} \mathbf{S}$$

where \mathbf{G} has elements, \mathbf{G}_{ik} . Consider a one-dimensional spectrum of i channels as being made up of the sum of line-shape functions $f_k(i)$ corresponding to the k constituents:

$$f_i(\mathbf{a}, i) = \sum_k a_k f_k(i) .$$

Then $f_i(\mathbf{a}, i)$ is a linear function of a_k for all k . All the non-linear terms are contained in $f_k(i)$. From the above it is clear that \mathbf{S} can be decomposed into the relative contributions from each constituent by applying the matrix transformation (eqn. 4) provided the line-shape functions $f_k(i)$ are known. The function $f_i(\mathbf{a}, i)$ is linear in its parameters a_k (which correspond to the yield associated with each lineshape) and thus the $\partial f_i(a, i) / \partial a_i$ terms are independent of \mathbf{a} . It follows from the linear combination of the different line-shapes (eqn. 5) that the matrix \mathbf{G} describes how much the channel contents S_i contribute to each a_k . Thus all counts from a channel S_i contribute to all component signals. The cross talk between the k th and $k-1$ th signal in regions where the separation is small leads to positive Γ_{ik-1} elements and this is corrected in a natural way by negative Γ_{ik-1} elements in regions where the separation of the signals is large.

For our particular application we are interested in decomposing the two dimensional mass number vs. energy spectrum into one-dimensional energy distributions for each component in the sample. The first step to achieve this was to re-bin the data into a series of one-dimensional mass-spectra corresponding to energy slices a single energy bin wide. Subsequently, for each individual energy slice in turn, the \mathbf{G} matrix was evaluated using line shapes $f_k(i)$ consisting of Gaussians where the centroid corresponded to the mass number A of the k th isotope and \mathbf{S} is given by the smooth monotonic function [24]:

$$\mathbf{s}(E, A) = C_1 + C_2 \frac{A^{3/2}}{E} + C_3 \frac{A^2}{E^{3/2}} + C_4 A E^{1/2} \quad (4)$$

where the constants C_1, C_2, C_3, C_4 were determined experimentally from a number of reference samples. Statistical weighting only weakly affects the convergence of the least squares fit [23]. If unity weights are employed, no assumption has to be made regarding the concentration of the different elements present in the sample and the \mathbf{b} and \mathbf{a} matrices (eqns. 2 and 3) become independent of a . If the lineshape functions are known, as in our case, it is a trivial task to obtain the $\mathbf{G} = \mathbf{a}^{-1} \mathbf{b}$ matrix and transform the \mathbf{S} to \mathbf{a} according to eqn. 4, and extract the amplitude a_k of the different components. These amplitudes are simultaneously assembled into one-dimensional energy spectra for all the components k by repeating the previous step for each energy bin.

The re-binning to a series of mass spectra that are fitted independently with equal weighting implies that this procedure requires no assumptions as to the energy distributions of the components, which we seek to measure. The only assumptions required are the mass-number position and lineshapes corresponding to the different recoil elements (isotopes) in the sample.

The method may be extended to directly fit two-dimensional ΔE vs. E and ToF vs. E spectra, or transformations of these, by making use of the property that the lineshapes for each recoil isotope follow a unique locus in $\Delta E, E$ and ToF, E space, respectively. These loci for each isotope and the corresponding lineshapes in the respective space can be uniquely determined using reference standards or appropriate empirical procedures, e.g. ref. 20-23.

3. Evaluation of the Method

The regime of Pt-In-I using 77 MeV I for ToF-E ERDA ions was used as an appropriate system to test the method, as it was a case of interest imposing significant practical difficulty. In order to investigate the suitability of the method for decomposing two-dimensional recoil mass-number vs. energy spectra we have employed both idealised simulated data, (where the energy distributions of components are known *a priori*) and experimentally measured data, (where the energy distribution of the components are to be determined).

3.1 Simulated tests

The simulated test data consisted of two-dimensional mass number vs. energy histograms that were generated energy-channel slice by slice from one-dimensional mass spectra. The one-dimensional mass spectra were comprised of superposed Gaussian mass-lineshapes with position and yield corresponding to the respective mass number and abundance of the recoil at the slice energy. The \mathbf{s} values were taken from equation 6 where the constants C_1, \dots, C_4 were determined for the experimental data used here from reference standards [24].

Fig. 1 shows the decomposed energy distributions from simulated rectangular energy spectra for three isotopes with $A = 102, 103$ and 104 , with respective and relative yield of 100:1:10. The recoil energy ranged from 15 to 38 MeV (channel 1000 to 2500). This corresponds to recoils from the greatest depth of interest to the surface, for the Pd/InP experimental data considered below. The mass-spectra of the simulated data are shown in Fig. 2 for the two extremes of the energy range. Typically, in the Pd-In-I region \mathbf{s} is ~ 2.3 u at the "surface" (38 MeV, channel 2500) and increases to ~ 3.4 u at the greatest depths (15 MeV, channel 1000). As can be seen from Fig. 1, in the limit of no disturbing influences, the agreement of the fitted distributions with the input data consisting of rectangular energy

distributions was excellent. The limited scatter in the minor isotope ($A = 103$) is associated with propagation of small numerical errors. This result confirms the numerical accuracy of the method.

In order to test the behaviour in the limit of low counting statistics, the simulated two dimensional spectrum described above was multiplied by a random factor obtained by counting a number corresponding to the yield, of pseudo-random numbers between 0 and 1 that exceed 0.5. Although not a correct model of a counting experiment, it provides a rapid test. Figure 3 shows the fitting result for same conditions as Fig. 1 but with simulated counting statistics, where the number of counts in the minor isotope signal is ~ 100 . The major isotope distribution ($A = 102$) is only weakly perturbed but already the second major distribution ($A = 104$) shows considerable scatter. For the minor isotope ($A = 103$) the statistical spreading even gives rise to negative values. Using the relative abundance 100:1:10, a series of tests showed it was necessary to have a separation in mass of about twice the \mathbf{s} value to obtain a distribution where the average value is in good agreement with the expectation value.

In a final test, the case of uniform rectangular energy distributions of ^{nat}Pd , ^{nat}In and ^{127}I , which corresponds to experimental test data from Pd/InP thin film structures, was investigated. The elemental yield ratios for Pd, In and I were taken to be 2:10:10, respectively, with a total ^{nat}Pd yield of 200 counts. Using Gaussian distributions to represent the isotope lineshapes and treating the abundance of the isotopes as free parameters, the different isotopic distributions exhibited wild fluctuations. However, the sum of the isotopic distributions was relatively smooth except at the lowest energies (Fig. 4a). In order to improve the situation the number of free parameters was reduced by

assigning the line-shape function $f_k(i)$ for each element rather than for each isotope:

$$f_k(i) = \sum_l V_l G(A_i, A_l, \mathbf{s}(A_l, E))$$

where \mathbf{z} is the product of the relative recoil cross-section and natural abundance of the l th isotope, A_i is the mass number assigned to mass channel number i , A_l is its mass number and $\mathbf{s}(A_l, E)$ the standard deviation of the Gaussian isotopic lineshape G from eqn. 6. In this case the a_k elements correspond to the content of the k th element, which reduces the number of free parameters. After this modification the agreement with the rectangular test data was found to be excellent (Fig. 4 b). Introducing counting statistics in the same manner as was done before led to mild fluctuations around the expectation yield value for Pd. (Fig. 4b). The considerable reduction in statistical scatter seen between Fig. 4 a and b, lead us to fit composite elemental line shapes (eqn. 7) in subsequent analysis of experimental data.

3.2 Experimental data

Figure 5 shows a contour plot of experimentally measured two-dimensional mass number vs. energy histogram in the Pd - In - I region. This data was obtained using a 77 MeV $^{127}\text{I}^{10+}$ ion beam from the ANTARES accelerator at Lucas Heights. The ion beam was incident at 60° to the surface normal and the recoils ejected at 45° to the beam direction were detected in a ToF-E detector telescope with a 437.5 mm flight length. The sample consisted of ~ 50 nm of Pd e-beam evaporated onto an (100) InP substrate [13,16,17]. In a typical ToF-E ERDA experiment data are collected with an ADC span of 4096 by 4096 channels. The relatively small number of counts, usually - 10^4 per measurement are generally associated with limited beam fluence and small detector telescope solid angle. The data were transformed to a two-dimensional mass energy spectrum following the procedure in ref. 10. In order to minimise effects of counting statistical uncertainties,

and speed up the calculations, the data were re-binned in mass and energy by merging channel contents to span the selected region of interest covering the Pd, In and I signals with 512 by 512 bins. The bin widths were chosen to be much smaller than the width of the features so that they have insignificant influence on the outcome of the fit. (Note that our software displays and handles the data in terms of the original channel number to avoid calibration difficulties.)

Fig. 6 represents the fitted Pd, In and ^{127}I signals from the data in Fig. 5. The shapes of the Pd, In and ^{127}I energy distributions agree very well with depth distributions obtained from gating on the signals when minimising the cross talk contributions from neighbouring elements [16]. Fig. 7 presents the fitted mass lineshapes corresponding to energy channel 2000 (Pd film) and channel 1000 (deep in the InP substrate). The thin surface layer of Pd was clearly resolved (Fig. 6 a). The In distribution (Fig. 6 b and Fig. 7 b) suggests that some In is present within the overlaying thin Pd film. X-ray diffraction studies [16] on the same sample showed no evidence of the formation of ordered Pd-In and Pd-P phases. Fig. 8 presents a depth profile corresponding to the same energy window using conventional gating and non-linear fitting procedures [16]. This suggests that a small quantity of In has indeed moved into the Pd layer. Moreover, there is evidence in the literature that Pd reacts with InP during deposition [25-27]. Fig. 7 b, which shows the fitted mass lineshape for an energy corresponding to the Pd layer, indicates there are significant areas under the Pd and In peaks where interference from neighbouring elements is negligible, (i.e. signals that are unique to Pd and In can be obtained). It follows that the conventional gating and fitting procedure used in refs. 11 and 16 should be reliable in the surface region. This implies that In is indeed present in the Pd film.

The Pd signal (Fig 6a) has a low energy tail, which becomes quite pronounced at the lowest energies. Tests revealed that the relative height of the tail was very sensitive to the mass calibration. A simulated change of 0.5 % in this parameter leads to significant changes in relative amplitude of the tail. The fitted mass spectrum corresponding to the Pd tail region, shown in Fig. 7 a, reveals that the size of the fitted peak corresponding to the Pd signal is very similar to the size of the low-mass tail of the fitted In lineshape. The contribution to Pd from the low mass tail of the ^{127}I signal is however, negligible. The fact that the amplitude of the deep Pd tail in Fig 6a is essentially zero between channels 1200 and 1800 and increases with decreasing energy below this interval, strongly suggests that the tail is purely an artefact of the fitting. Further evidence of this is seen in Fig. 8 which shows for the same data, the depth distribution of Pd obtained using judicious gating based on non-linear fitting [16] to select the Pd signal only from a mass region where interference from In is minimal. This analysis of the same sample shows no evidence of a tail in the Pd distribution. (Fig. 8.) The Pd deep tail can thus be associated with uncertainty in the mass calibration and deviations of the low mass tail of the In lineshape from the $f_k(i)$ calculated using Gaussian isotopic lineshape functions G in equation 7. It has previously been shown [24] that the isotope lineshapes are described well by a Gaussian distribution for light (^{12}C , ^{16}O) and medium heavy ($^{69,71}\text{Ga}$, ^{75}As) isotopes. The mass resolution is dominated by the contribution from the Si detector [28] and no deviation from a Gaussian behaviour is anticipated for heavier recoils. The most likely origin of the tail is therefore the progressive shift in the energy, (and hence mass) calibration resulting from radiation damage of the Si energy detector [29] that occurred between the measurements to establish the mass calibration and the measurements of the data used here.

4. Discussion and Conclusions

The statistical analysis method requires the line shape and position to be accurately known in order to fit the spectrum with an analytical function representing this line shape. The assignment of a line shape function to each element instead of each isotope is preferred because this minimises uncertainties associated with counting statistics and numerical rounding errors. In principle, isotope line shapes should be fitted because they are uniquely defined. Practice has shown the method can be difficult to apply for isotope line-shapes in the present study, probably due to inadequacies in mass calibration. The assumption of a single line-shape function for each element has a drawback in that the energy signals from different isotopes are displaced in energy because of the different kinematic factors and stopping powers associated with the different isotopes. Another approach is to use reference standards to directly determine $f_k(i)$ for each element of interest. In this case the transformation from ToF vs. E is unnecessary, which considerably simplifies the analysis. (The situation is slightly more complex in the case of ΔE - E ERDA because it will be necessary to calculate the total energy of the recoil from the ΔE and E signals.)

The nature of the method implies that the $f_k(i)$ functions used for the spectral decomposition have to be established accurately [23] otherwise uncertainties will be introduced into the elemental distributions. Calibration shifts associated with radiation damage of Si detectors [29] used in ToF-E ERDA are problematic in this respect. Although computationally tedious, these can be corrected by interpolation between calibrations established at regular intervals [29]. Alternatively, gas ionisation detectors, which are insensitive to the cumulative effects of radiation damage, can be employed. *It follows, that when a Si energy*

detector is used for ToF-ERDA analysis, decomposition of mass overlapped energy spectra based on a non-linear fitting procedure is superior to the present method. This is because by treating the mass calibration parameters as free in the final iteration stages, small variations in the parameters can be compensated.

It may be plainly seen from the data in Figures 5-8 that the method functions well in the high energy limit where the overlap between elemental signals is small and the form of the lineshapes varies slowly with energy. With progressively lower recoil energies the uncertainties in the mass lineshape and mass calibration increasingly manifest themselves as an increased cross talk between elemental signals and increased fluctuations in the fitted elemental signals.

Provided the mass calibration can be controlled, the computationally tedious determination of the transformation matrix **G** (eqn. 4) need only be done once. Then the yields for each element are obtained by a simple matrix multiplication. This makes the method particularly well suited where a number of components are to be decomposed from overlapping spectra corresponding to closely similar samples as well as for direct on-line data analysis for standard routine analysis.

Acknowledgements

The authors would like to thank Chris Ryan for valuable discussions regarding the method. The Swedish authors would also like to acknowledge Carl Trygger's Foundation and The Royal Physiographical Society of Sweden for financial support.

References

[1] H.J. Whitlow, M. Andersson, M. Hult, L. Persson, M. El Bouanani, M. Östling, N. Lundberg, D.D. Cohen, N. Dytlewski, P. N. Johnston, I.F. Bubb, S.R. Walker, E. Johanson, S. Hogmark and P. A. Ingemarsson, Mikrochim. Acta 120 (1995)171.

[2] Y. Zhang, M. Elfman, T. Winzell, H.J. Whitlow, Nucl. Instrum. Meth. B 150(1999)548.

[3] T. Winzell, Y. Zhang, H.J. Whitlow, Nucl. Instrum. Meth. B 161-163(2000)558.

[4] Y. Zhang, G. Possnert, L. Jonsson, T. Winzell and H.J. Whitlow, Proc. 4th Int. Conf. Thin Film Physics and Applications, Shanghai, China, May 2000, SPIE Press. (Submitted.)

[5] A. G. Seamster, R. E. L. Green, and R. G. Korteling. Nucl. Instr. and Meth., 145(1977) 583.

[6] L. del Peral, J. Mednia, and E. Bronchalo. Nucl. Instr. and Meth., A348(1994)192.

[7] M. El Bouanani, P. N. Johnston, I. F. Bubb, and H. J. Whitlow. CP392, *Applications of Accelerators in Research and Industry*, (eds.) J.L. Duggan and I.L. Morgan (AIP Press, New York, 1997) 674.

[8] H.J. Whitlow, T. Winzell and G. Thungström, Nucl. Instr. Meth. B136(1999)616.

[9] Y. Zhang, T. Winzell and H.J. Whitlow, Nucl. Instr. Meth. B159(1999)101.

[10] M. El Bouanani, M. Hult, L. Persson, E. Swietlicki, M. Andersson, M. Östling, N. Lundberg, C. Zaring, D. D. Cohen, N. Dytlewski, P. N. Johnston, S. R. Walker, I. F. Bubb, and H. J. Whitlow. Nucl. Instr. and Meth., B94(1994)530.

[11] M. Hult, H. J. Whitlow, and M. Östling. Appl. Phys. Lett., 60(1992)219.

[12] M. Hult, H. J. Whitlow, M. Östling, M. Andersson, Y. Andersson, I. Lindeberg, and K. Ståhl. J. Appl. Phys., 75(1994)835.

[13] L. Persson, M. Hult, H. J. Whitlow, M. El Bouanani, M. Andersson, I. F. Bubb, P. N. Johnston, S. R. Walker, D. D. Cohen, N. Dytlewski, N. Lundberg, C. Zarnig, and M. Östling. In: P. Misaelides, editor, *Application of Particle and Laser Beams in Materials Technology*. (Kluwer Publications, 1995) p. 471.

[14] H. J. Whitlow, M. Andersson, M. Hult, L. Persson, M. El Bouanani, M. Östling, C. Zaring, N. Lundberg, D. D. Cohen, N. Dytlewski, P. N. Johnston, I. F. Bubb, and S. R. Walker. Vacuum, 46(1995)737.

[15] R. Ghetti, B. Jakobsson, and H. J. Whitlow. Nucl. Instr. Meth. A317(1992)235.

[16] L. Persson, M. El Bouanani, M. Hult, P. Jönsson, H. J. Whitlow, M. Andersson, K. Georgsson, I.F. Bubb, P. N. Johnston, S. R. Walker, D. D. Cohen, N. Dytlewski, C. Zaring, and M. Östling. J. Vac. Sci. Techn., A14(1996)2405.

[17] L. Persson, M. El Bouanani, M. Hult, P. Jönsson, H. J. Whitlow, M. Andersson, K. Georgsson, I.F. Bubb, P. N. Johnston, S. R. Walker, D. D. Cohen, N. Dytlewski, C. Zaring, and M. Östling. J. Appl. Phys., 80(1996)3346.

[18] L. Persson. *Ion beam characterisation of nanometre structures*. PhD thesis, Lund Institute of Technology, 1995.

[19] P.N. Johnston, M. El Bouanani, W.B. Stannard, I.F. Bubb, P. Jönsson, Y. Zhang and H.J. Whitlow, CP392, *Applications of*

- Accelerators in Research and Industry*, (eds.) J.L. Duggan and I.L. Morgan (AIP Press, New York, 1997) 715.
- [20] C. G. Ryan, D. N. Jamieson. *Nucl. Instr. and Meth.*, B77(1993)203.
- [21] C. G. Ryan, D. N. Jamieson, C. L. Churms, and J. V. Pilcher. *Nucl. Instr. and Meth.*, B104(1995)157.
- [22] C.G. Ryan, E. van Achterbergh, D.N. Jamieson, and C.L. Churms. *Nucl. Instr. and Meth B* 109-110 (1996)154.
- [23] E. Clayton and C. G. Ryan. *Nucl. Instr. and Meth.*, B49(1990)161.
- [24] M. Hult, M. El Bouanani, L. Persson, H. J. Whitlow, M. Andersson, C. Zaring, M. Östling, D. D. Cohen, N. Dytlewski, I. F. Bubb, P. N. Johnston, and S. R. Walker. *Nucl. Instr. and Meth.*, B101(1995)263.
- [25] M. Andersson-Söderberg, Comprehensive summaries of Uppsala dissertations from the Faculty of Science (1992) paper VI.
- [26] R. Caron-Popowich, J. Washburn, T. Sands, A.S. Kaplan, *J. Appl. Phys.* 64(1988)4909.
- [27] D.G. Ivey, P. Jian, and R. Bruce, *J. Electron. Mater.* 21(1992)831.
- [28] H.J. Whitlow, B. Jakobsson and L. Westerberg, *Nucl. Instrum. Meth.* A310(1991)636.
- [29] Y. Zhang, H.J. Whitlow, T. Winzell, *Nucl. Instr. Meth. B* 161-163 (2000)297.

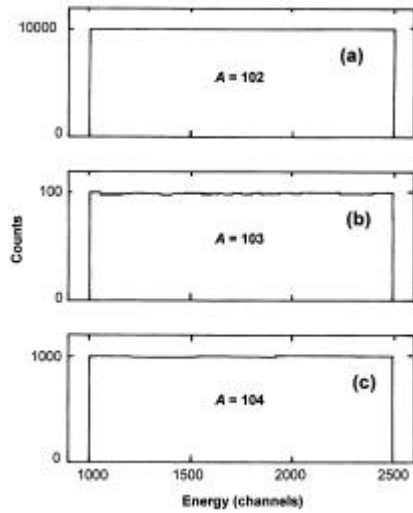


Fig. 1 The decomposed energy distributions obtained using Gaussian distributions without counting statistical spreading as test data. The relative abundances between $A = 102$ (a), $A = 103$ (b) and $A = 104$ (c), were 100:1:10.

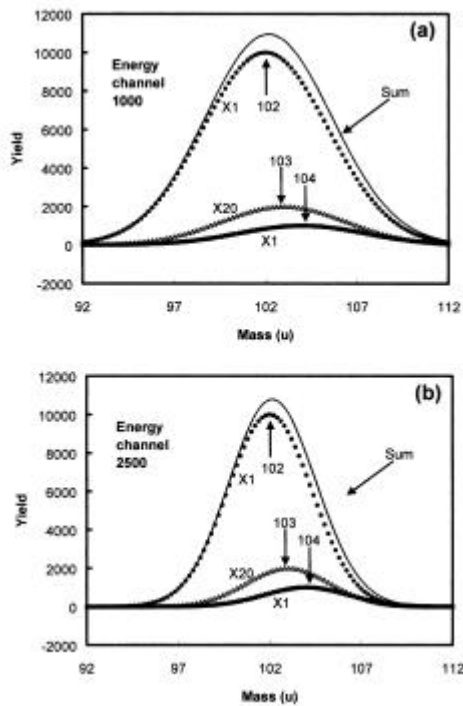


Fig. 2 Mass lineshapes for the test data used in Fig. 1 at (a) lowest energy 15 MeV (b) highest energy 38 MeV. For clarity the amplitude of the signal for $A = 103$ has been magnified.

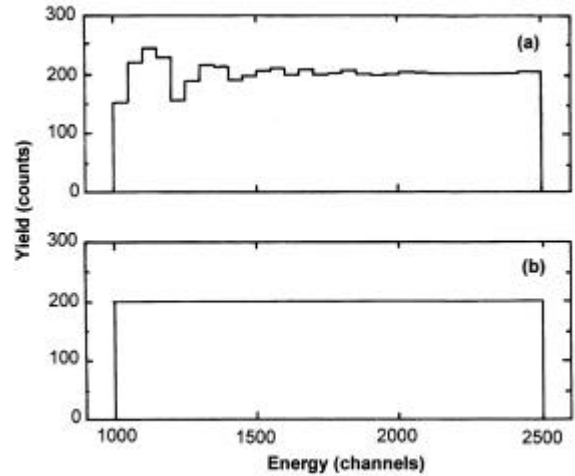


Fig. 3 Decomposed energy distributions as for Fig. 1 where simulated counting statistics have been introduced. (a) $A = 102$, (b) $A = 103$, (c) $A = 104$.

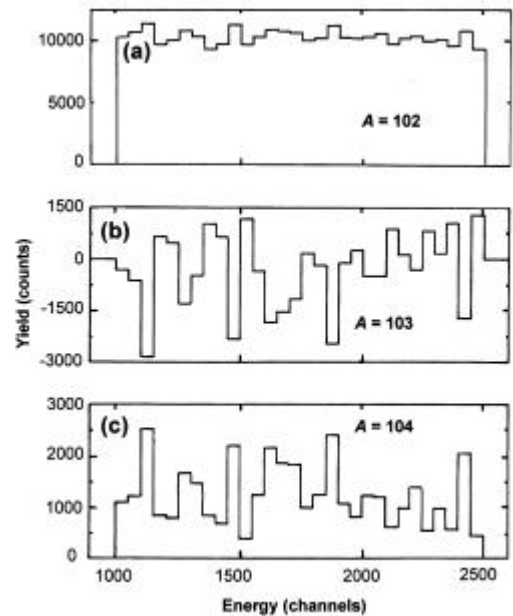


Fig. 4 (a) The sum of fitted total signal yields from all Pd isotopes when a single Gaussian lineshape function is fitted independently for each isotope. (b) The fitted Pd total signal yield when a composite lineshape (eqn. 7) comprising Gaussians corresponding to the natural abundance and mass of each Pd isotope was fitted.

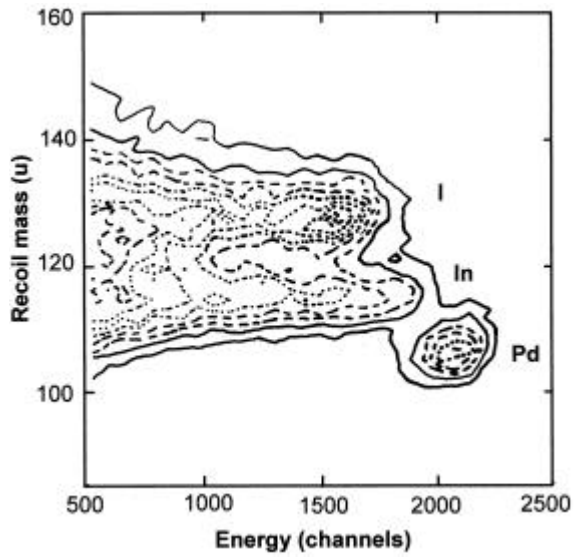


Fig. 5 Mass number vs. energy contour plot for 50 nm Pd/InP in the Pd-In-I region. The contour lines are drawn at ten equally spaced yield intervals.

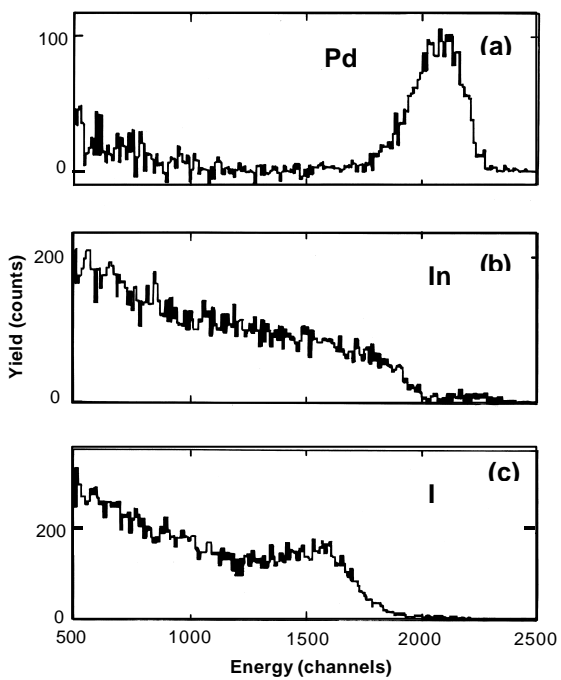


Fig. 6 Fitted elemental energy distributions from the data of Fig. 5 for (a) ^{nat}Pd , (b) ^{nat}In and (c) ^{127}I .

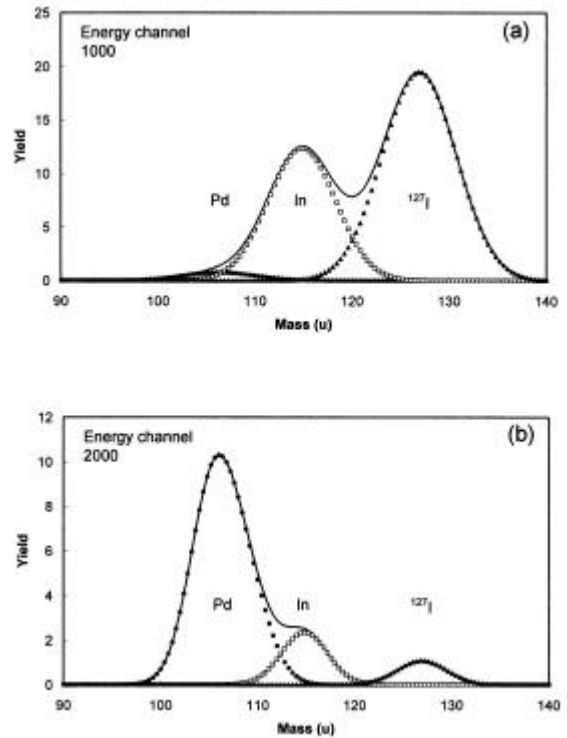


Fig. 7 Fitted mass lineshapes corresponding to the data in Figs. 5 and 6 for energy channels in the (a) InP substrate and (b) Pd surface film. The elemental lineshapes $f_k(i)$ were calculated according to eqn. 7.

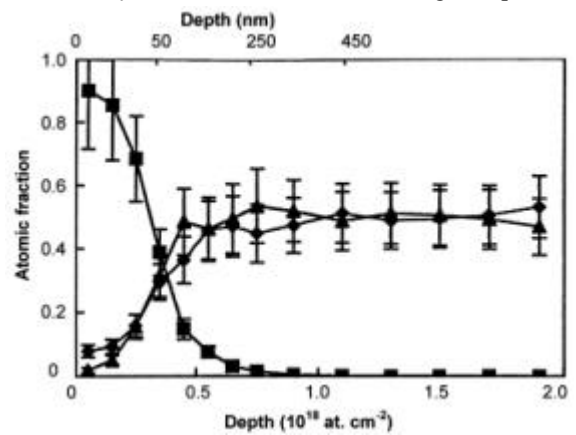


Fig. 8 Depth distribution from the Pd/InP sample data (Fig. 5) determined using a combination of non-linear fitting and gating [16]. The triangles, diamonds and squares denote P, in and Pd, respectively. The error bars indicate the total uncertainty, which is dominated by the contribution from the stopping cross sections.